ACS APPLIED MATERIALS & INTERFACES

RESEARCH ARTICLE

www.acsami.org

Brush-Shaped ZnO Heteronanorods Synthesized Using Thermal-Assisted Pulsed Laser Deposition

Jaewan Choi,[†] Hyunjin Ji,[†] Octolia Togibasa Tambunan,[§] In-Sung Hwang,[‡] Hyung-Sik Woo,[‡] Jong-Heun Lee,[‡] Bo Wha Lee,[§] Chunli Liu,[§] Seuk Joo Rhee,[§] Chang Uk Jung,[*,§] and Gyu-Tae Kim[*,†]

[†]School of Electrical Engineering and [‡]Department of Materials Science and Engineering, Korea University, Seoul, 136-713, Korea

[§]Department of Physics, Hankuk University of Foreign Studies, Gyeonggi-do, 449-791, Korea

Supporting Information

ABSTRACT: Brush-shaped ZnO heteronanostructures were synthesized using a newly designed thermal-assisted pulsed laser deposition (T-PLD) system that combines the advantages of pulsed laser deposition (PLD) and a hot furnace system. Branched ZnO nanostructures were successfully grown onto CVD-grown backbone nanowires by T-PLD. Although ZnO growth at 300 °C resulted in core−shell structures, brush-shaped hierarchical nanostructures were formed at 500−600 °C. Materials properties were studied via photoluminescence (PL), scanning electron microscopy (SEM) and transmission electron microscopy (TEM) characterizations. The enhanced photocurrent of a SnO_2−ZnO heterostructures device by irradiation with 365 nm wavelength ultraviolet (UV) light was also investigated by the current−voltage characteristics.

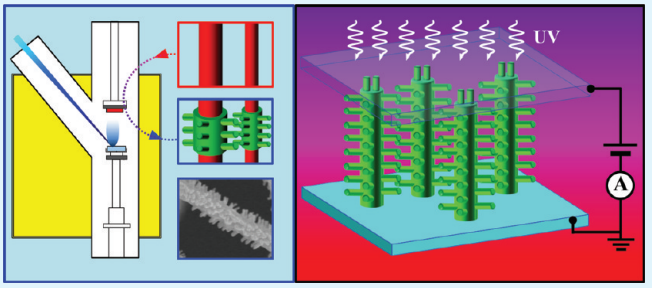

KEYWORDS: brush-shaped heteronanostructures, thermal-assisted pulsed laser deposition, photocurrent

ZnO in group II−VI is a generally n-type semiconductor because of Zn interstitials or oxygen vacancies that can generate extra free electrons in the channel. Crystalline ZnO has a Wurtzite structure with lattice parameters of a = 3.2495 Å and c = 5.2069 Å. Because of its wide direct band gap energy (3.3 eV) and its large exciton binding energy (about 60 meV[1−3]), its applicability to optoelectronics has been demonstrated in photoconductors, photodiodes, and phototransistors. Further interest in ZnO materials has expanded from simple nanorod, nanowire, and nanoribbon structures to more complicated structures such as core−shell and hierarchical structures. Nanoscaled hybrids have substantial structural benefits that maximize the active area of sensors or lead to a high integration of nano p−n diodes for a high efficiency, as reported by Lieber et al.[4] Recently, heterostructures utilizing two or more kinds of metal oxide nanomaterials that surround the backbone nanowires have been prepared through vapor transport and condensation techniques.[5,6] Self-assembled branched nanostructures can also be formed by (1) high-temperature thermal evaporation of precursor powders, (2) multiple vapor−liquid−solid (VLS) growths by reseeding the nanowire surface with catalytic nanoparticles, and (3) a sol−gel process of metal oxide materials, as reported by Fan et al.[7] However, the above-mentioned methods have several problems that need to be solved, such as limited choice of materials, complex processes, poor reproducibility, and poor physical properties of the products.

There are various techniques generally used to fabricate ZnO nanostructures. These include chemical vapor deposition (CVD), thermal evaporation, sol−gel process, and sputtering. However, the pulsed laser deposition (PLD) technique has typically resulted in the best physical properties for the grown ZnO nanostructures because the high energy of a pulsed laser can provide a more stable source of a ZnO plume compared to other methods. There is also an efficient transfer of activated ZnO particles to the proper sites during the laser off-time, resulting in formation of a highly crystalline film.[8,9] To achieve the better quality of nanostructures by PLD, it is needed to be developed the limitations such as the heat loss caused by the temperature gradient between the target and the substrate, and the supply of oxygen to a small space rather than the entire reactive area.

Several research groups have tried to create nanostructures using the pulsed laser deposition method with a hot furnace system having a horizontal quartz tube inside to control the overall environmental temperature in the reactive area.[10−12] When materials are grown by pulsed laser deposition, the stable plasma plume with a fixed direction and a shape is the most important factor and it is significantly affected by the flatness of the target surface. To compensate the deficiencies in the existing combination systems of PLD and a furnace, we have devised a new thermal-assisted PLD (T-PLD) system. This system has three advantages; two advances compared with the existing combination systems of a vertical Y-shaped tube and a rotating

Received: August 17, 2011
Accepted: November 4, 2011
Published: November 04, 2011

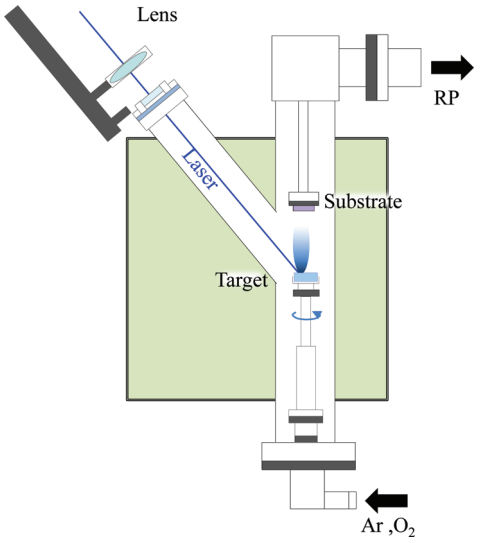

Figure 1. Thermal-assisted pulsed laser deposition system.

target system, and one advance compared with the conventional PLD method of a hot-furnace. It is oriented with a vertical Y-shaped quartz tube which not only enables to make a stable and uniform plume at a right angle to the substrate, but also gives very consistent gas flow along the tube. And it can heat the entire reaction zone due to the hot furnace system which could cover the target and the substrate completely. Finally, its rotating target holder is very advantageous in providing a constant plume shape. Rastering the focused laser over a wider target surface provides uniform shape and direction of the plume and maintains the flatness of the target surface for a much longer time. In this study, a two-step growth method has been used with our T-PLD system to create brush-shaped ZnO heteronanostructures around CVD-grown backbone nanowires. The objective was to create sensitive nanostructures for use as photodetectors. The hierarchical structures are particularly advantageous for chemical sensors because of their large reactive surface areas. Furthermore, the hierarchical structures can be applied to photocatalysts with a tunable energy band. The energy band configurations also can be engineered for general optoelectronic devices such as solar cells or p-n junction diodes with the different heterogeneous cores or outer materials. The photoresponses of these SnO_2−ZnO hierarchical structures were measured to demonstrate their suitability for prospective optoelectronic devices.[7]

A ZnO (99.99% pure) solid target of 1 in. diameter and a heavily doped Si substrate were placed inside the furnace (Figure 1). In contrast to conventional PLD systems, a vertical Y-shaped quartz tube and a rotating target holder were adopted to produce a uniform plasma plume. This is because the shape and direction of a plasma plume produced by hitting a target with a high-energy focused pulsed laser is strongly affected by the morphology of the target surface. Some groups have used a straight quartz tube in line with a pumping system installed on a horizontal table; this is unstable and causes irregular plasma plumes because the surface of the target is roughened as a result of being continuously struck by the focused pulsed laser beam.[12] In our T-PLD system, a pulsed KrF excimer laser (λ = 248 nm, 8 Hz, 2−3 J/cm^2) was used to produce the plasma plume directed from the ZnO target onto the Si substrate. This substrate had a 3 nm Au layer as a catalyst on the top surface. The nanocluster plume created by the pulsed laser was formed at a right angle to the substrate surface and the target stage was rotated at a speed of 10−30 rpm. The environmental temperature inside the furnace was changed with heating coils close to the tube area and in situ controlled by the computer. Pure Ar and O_2 gases at constant flow rates of 200 and 1 sccm, respectively, were injected into the quartz tube. A constant pressure of 1.2 Torr inside the tube was maintained by keeping a balance between the flow rates of injected gases controlled by mass flow controllers (MFC) and the pumping rate by a rotary pump. The ambient temperature for producing the nanostructures in this T-PLD was varied from 200 to 700 °C. The optimum furnace temperature of 600 °C is quite low compared to the temperatures used in other synthesis methods to fabricate nanostructures. The distance from the substrate to the target was adjusted between 3 and 6 cm in the T-PLD system.

ZnO was selected for producing the hierarchical nanostructures over Si or SnO_2 nanowires. The combination of a Si nanowire core with an outer ZnO nanostructure is interesting from the point of view of nanoscale p-n junction devices such as nanowires grown on Si substrates.[5] First we studied the growth conditions of the one-step T-PLD growth for ZnO nanomaterials. And based on the experimental results of the one-step growth, the growth conditions were changed for the optimization of the formation of the hierarchical nanostructures; the ambient temperature, the pressure, and the laser conditions. And ultimately the optimal synthesis conditions were identically determined in both of the one-step growth and the branched growth of ZnO materials. The ambient temperature was considered to be the most critical point in producing the nanostructures than the other conditions.

The structural morphologies of the ZnO nanostructures grown by the one-step T-PLD were characterized using field-emission scanning electron microscopy (FE-SEM, Hitachi S-4300) and transmission electron microscopy (TEM, JEM-2100F). The room temperature photoluminescence (PL, SPEX 1702/04) measurements of the ZnO nanostructures synthesized under various ambient temperatures were performed using the 325 nm line of a continuous HeCd laser as an excitation source. And the temperature-dependent PL was measured from 10 to 300 K for the ZnO nanoneedles optimally grown at 600 °C in detail. Electrical properties were measured using a semiconductor parameter analyzer (HP 4145B). Field-effect transistors (FETs) using single, individual ZnO nanorods were fabricated by a conventional electron beam lithography technique,[13] metal deposition, and a lift-off process. First, ZnO nanorods dispersed in an isopropyl solution were dropped onto a Si/SiO_2 substrate (300 nm oxide thickness), and then a poly(methyl methacrylate) electron resist solution was uniformly spin-coated over the substrate as a thin film. After designing the electrode patterns using our own design program, the sample was exposed to an electron beam selectively and the development was processed using a methyl isobutyl ketone solution (MIBK:IPA = 1:3). Considering the n-type nature of ZnO and matching of the Fermi levels, it was evaporated of Ti/Au (20/150 nm) as a top electrode and followed a lift-off process in acetone solution. To ensure ohmic contact between the metal electrodes and the ZnO channel, rapid thermal annealing (RTA) was carried out for 5 min at 400 °C under ambient nitrogen gas. Electrical probing was done using a micropositioning system; the current−voltage characteristics were measured using a voltage source and a pico-ammeter. The photocurrents of the hierarchical nanostructures

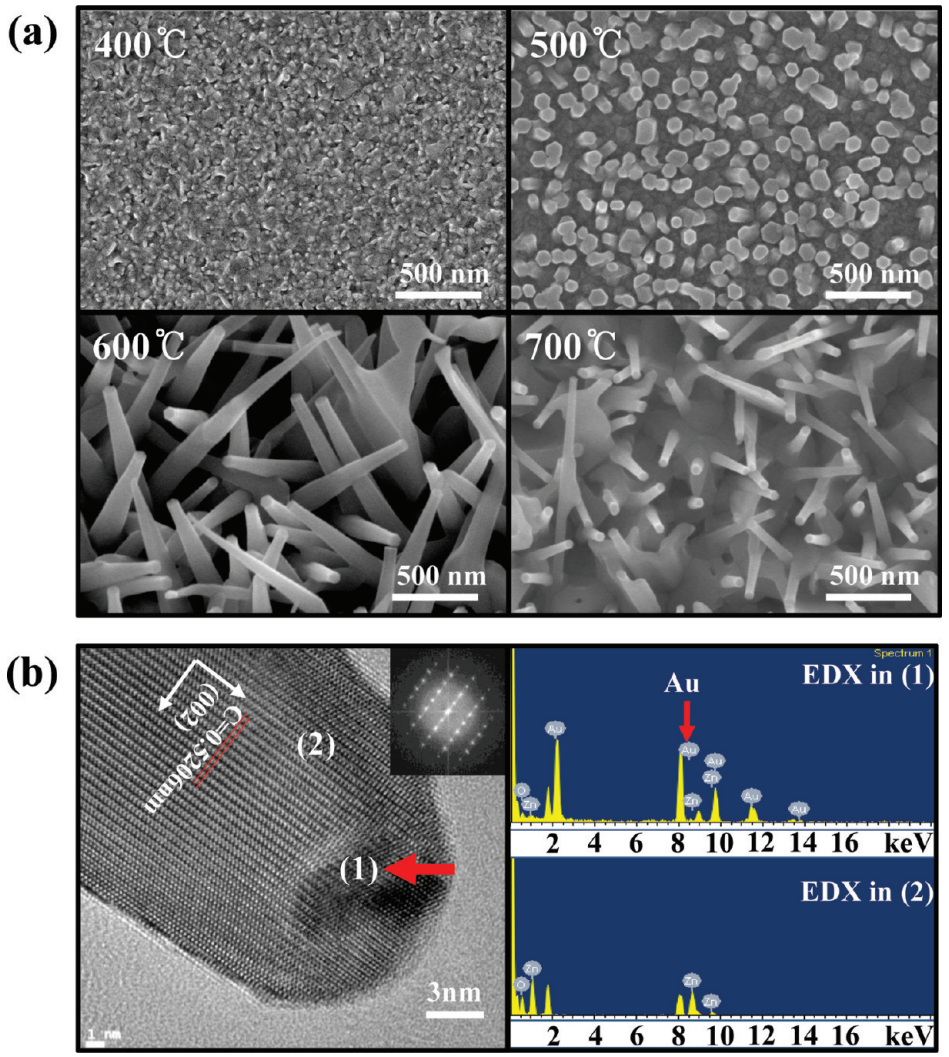

Figure 2. (a) SEM images of the ZnO nanostructures synthesized using the T-PLD method at different temperatures. (b) High-magnification TEM image of the ZnO nanoneedle synthesized at 600 °C by T-PLD and the EDX analyses in ZnO body and tip materials (inset : the FT pattern from the selected area).

were measured with transparent top electrodes in a sandwich configuration as schematically shown in Figure 6a. The upper electrode was prepared using a transparent indium−tin-oxide (ITO) conducting glass; the bottom of the heavily doped Si substrate used as the counter electrode. In the photocurrent measurement, an ultraviolet (UV) lamp with a wavelength of 365 nm was used. It was also shown in the right side of Figure 6a as real photograph images.

Figure 2 shows the morphology of the ZnO nanomaterials synthesized at different temperatures on the heavily doped Si substrate with Au catalyst. To characterize the influence of the thermal energy on the change of ZnO nanomaterials morphology, when they were fabricated by T-PLD, we varied the growth temperature from 200 to 700 °C. At lower temperatures, a film structure formed predominantly (see Figure S1 in the the Supporting Information for all SEM images). As the temperature increased closer to 600 °C (Figure 2a), the shape of nanoneedle became prominent. The shapes of the deposited ZnO materials were mainly determined by the kinetic energy of the ZnO feedstock. This energy was originated from both the environmental thermal energy in the furnace and momentum transfer by the pulsed laser. Different to the conventional PLD system, the pulsed laser and the hot furnace provide together the kinetic energy enough to create nanostructures on the substrate by the high energy of the plasma plume away from the ZnO target surface in T-PLD. Below 500 °C, neighboring nucleated particles predominantly formed layer-by-layer assemblies, resulting in a ZnO film. The lack of thermal energy from the furnace resulted in the textured films composed of ZnO grains as shown in Figure 2 (the structures grown at 200,300 °C can be checked in Figure S1 in the Supporting Information). As the growth temperature increased from 200 to 400 °C, the grain size of the film increased. Even slightly above 500 °C, not far from the melting point of Zn (T_{melt} = 419 °C), the ZnO materials took the form of nanostructures growing along the *c*-axis.[14] However, the thermal energy of 500 °C does not seem to be enough for the formation of ZnO nanostructures, which could not identify the nanostructures from the points of the lengths and diameters. Needlelike structures were evident at 600 °C; their mean lengths and tip diameters were around 2 μm and 50−100 nm, respectively. The nanostructures were seemed to be grown from an initial ZnO buffer layer and resulted in the nanoneedle shaped structures

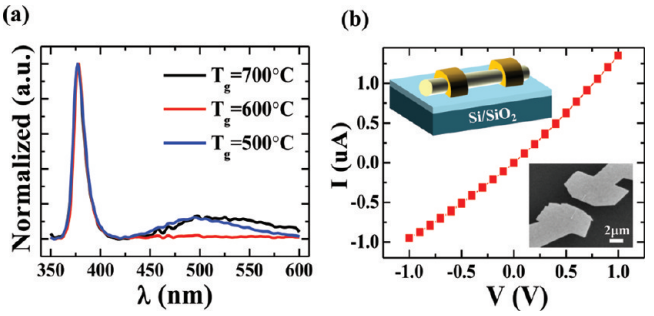

Figure 3. Room-temperature PL properties of the ZnO structures synthesized at different temperatures (500, 600, 700 °C) using the T-PLD technique. (b) Voltage−current characteristics of individual ZnO nanoneedle device synthesized at 600 °C (insets: the SEM image and schematic of the device).

which can be easily nucleated by merging into a rough morphological surface like a seed layer as following the VLS mechanism as verified in the Figure 2b with TEM image of Au particles on the tip of the nanostructures.[15,16] It was investigated in detail that the materials properties with TEM and SEM in Figure 2b for ZnO nanoneedle shaped structures grown at 600 °C by T-PLD. So High resolution TEM (HR-TEM) analyses established that the ZnO nanoneedles grew in a Wurtzite structure along the *c*-axis with lattice parameters $c = 0.5206$ nm in the (002) direction and $a = 0.329$ nm in the (010) direction. When the ZnO nanostructures were synthesized in a simple one-step growth using T-PLD, the growth mechanism followed the VLS process, as verified by energy dispersive X-ray spectroscopy (EDX) analysis. The reactants formed by the pulsed laser from the ZnO target developed nanostructures as they changed the state from liquid to solid in the heated Au catalyst. This was supported by EDX analysis that showed Au remaining in the top of the ZnO nanoneedles. Above 700 °C, additional activated particles were merged to the nanoneedles and resulted in the fan-shaped structures as shown in the Figure 2a of the SEM image for 700 °C.

In Figure 3, the three kinds of ZnO nanostructures grown by T-PLD were compared with PL results which were considered as the more distinguishable nanostructures and with the evident growth direction to (001) than the others; ZnO structures grown at 500,600 and 700 °C. (In Figure S2 in the Supporting Information, it was also shown the PL properties and XRD analyses of all ZnO structures grown at 200−700 °C for comparison.) The PL intensity of the band-edge emission (λ = 380 nm) for the ZnO structures synthesized below 400 °C was much smaller than those of the ZnO structures synthesized at higher temperatures (see Figure S2 in the Supporting Information). This was due to insufficient thermal energy in the growth of ZnO structures for the stable stoichiometry. When the growth temperature increased above 400 °C, sufficient thermal energy began to be provided for chemically combining the Zn particles with the oxygen molecules stable. The band-edge emission was produced from radiative excitons of ZnO lattices but the comparative intensities of PL results cannot represent the degree of the crystalinity. So the normalized results of band edge emission were shown in Figure 3a) for an easier comparison of the green emission in the samples grown above 500 °C. In ZnO materials, the green emission at around λ = 500 nm was shown due to oxygen vacancies or Zn interstitials. The ZnO structures

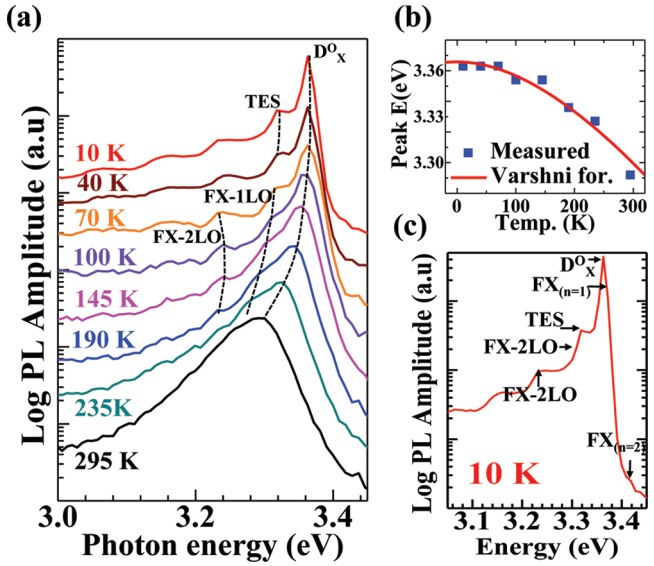

Figure 4. PL results for ZnO nanoneedles grown at 600 °C by T-PLD: (a) temperature-dependent PL properties for the UV region; (b) peak energy-dependent temperature as fitting to Varshni formula; (c) PL spectra in UV region measured at 10 K (magnified from a).

synthesized at 600 °C shows further low intensity in the green emission than the structures grown at 500 or 700 °C as indicating the better quality of the lattice crystal. The reason of the poor crystalinity in the sample made at 700 °C than that in 600 °C could be explained by that the increased supply of Zn atoms rather induced the Zn-rich phase in the ZnO structures as degrading the stochiometry because the melting point of Zn is around 419 °C. The degraded stochiometry in the sample of 700 °C was shown in a PL result with quite oxygen defects.[17,18] The tendency of the materials properties by PL characterization was also analyzed with the full-width at half-maximum (fwhm) which decreased as the growth temperature increased (shown in Figure S2a in the Supporting Information in detail). Taken together of the results in SEM, TEM, PL, and XRD measurements, the optimal formation of ZnO nanostructures was found in the growth at 600 °C by T-PLD.

To obtain a detailed characterization of the ZnO nanomaterials grown at 600 °C, low-temperature PL measurements were performed, as shown in Figure 4. Low-temperature PL measurements reduce the effect of phonon-scattering that can blur the observation of the intrinsic material properties. The band gap energy was decreasing with increasing of the ambient temperature due to the electron−phonon interaction and the expansion of the lattice. As shown in Figure 4b, the main peak (λ = 380 nm) of the ZnO structure shifted to 3.36 eV at 10 K from 3.29 eV at 295 K, indicating a crystalline structure of the ZnO. The shift of the peak energy position was fitted to Varshni formula of eq 1 as showing the consistent tendency and the parameters were found as $E(0) = 3.366$ eV, $\alpha = 0.008$ eV/K, $\beta = 790$ K.[19] $E(T)$ indicates the band gap energy at a temperature of T (so, $E(0)$ means the band gap energy at 0 K) and α, β are the constants.

$$E(T) = E(0) - \frac{\alpha T^2}{T + \beta} \quad (1)$$

Several of the PL peaks at T = 10 K were identified as the ground-state free excitons ($FX_{(n=1)}$), the first excited state ($FX_{(n=2)}$), the

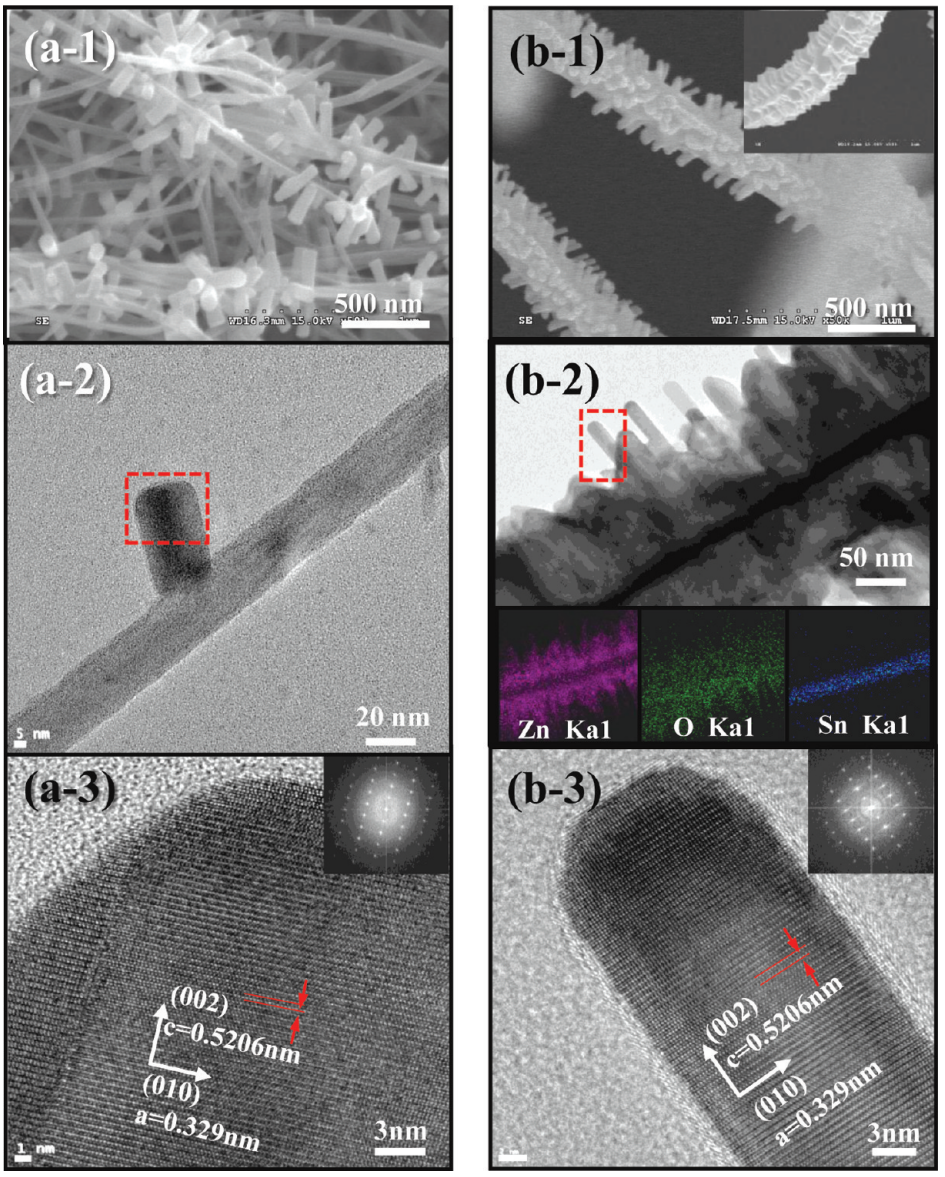

Figure 5. SEM images of the hierarchical structures with the secondary grown ZnO branches on: (a) Si and (b) SnO_2 backbone nanowires formed in advance by T-PLD (branches) and CVD (backbone) techniques (inset of b: excessively long 2nd ZnO growth results in the aggregation of ZnO materials). (c) Low-magnification TEM image of the Si-ZnO hierarchical structure. (d) Low-magnification TEM image and EDX analyses of the SnO2-ZnO hierarchical structure. (e, f) High-magnification TEM images and FT patterns in each sample show the crystalline ZnO branches.

free excitons bound to neutral donors (D^O_X), and their two-electron satellite transitions (TES) at FX-1LO (longitudinal-optical) and FX-2LO. These were indistinguishable at room temperature because of their low intensities or their overlap with adjacent peaks. Thermal dissociation can lead to a gradual disappearance of the D^O_X and TES LO phonon replica emissions due to the lower binding energy, as seen at higher temperatures. At T = 10 K, all the PL peaks were separated to $FX_{(n=1)}$, $FX_{(n=2)}$, D^O_X, TES, FX-1LO, and FX-2LO at 3.372, 3.420, 3.363, 3.318, 3.307, and 3.232 eV, respectively. The FX-1LO and FX-2LO peaks were thermally broadened and red-shifted as the ambient temperature increased. The physical parameters of $FX_{(n=1)}$, FX-1LO, and FX-2LO were calculated according to the equation presented in the Supporting Information (Figure S3), confirming the good quality of the crystals synthesized using our T-PLD techniques. The binding energy, R, of the ZnO nanoneedles was evaluated using the Lorentzian fitting equation $[E_n = E_g - (R/(n^2))$ $(n = 1,2,3,...)]$ and was calculated to be 58 meV at 10 K, very close to the reported value of 60 meV.[3,20]

From the ZnO nanoneedles grown at 600 °C by T-PLD, the individual ZnO nanoneedle device was fabricated as represented in the insets of Figure 3b as following the conventional electron beam lithography technique explained in detail previously. The electrical property of the individual ZnO nanoneedle was measured, as shown in Figure 3b. The nearly linear current−voltage characteristics had a high conductance, indicating a high carrier concentration of a ZnO nanoneedle obtained through our T-PLD method.

As mentioned earlier, the T-PLD system can be advantageous for growing various structures with different metal oxide nanomaterials due to the easier transfer of various materials with the pulsed laser as a plasma plum. The two-step hybrid growth of

metal oxide materials by T-PLD was implemented based on the results from the simple ZnO structure growth by T-PLD. When the ZnO materials were deposited by T-PLD as a second step below 300 °C onto existing nanowires, film-shaped layers were formed as the core−shell structures (the SEM images can be seen in Figure S4 in the Supporting Information). As temperature increased above 500 °C with a backbone of Si nanowires, the two-step growth produced branched hierarchical structures, as shown in Figure 5a-1, which look similar to brushes. The use of SnO_2 nanowires as a backbone for our two-step growth process also showed similar shapes as the Si-ZnO hierarchical structures in Figure 5b-1. The large surface of four facets of the rutile SnO_2 nanowires was more advantageous for the hierarchical ZnO structures formation. The more uniform brush shaped hierarchical structures were formed into SnO_2 core nanowires with the ZnO materials at the T-PLD growth temperature of 500 °C for 15 min. The poor uniformity of the protruding structures from the Si backbone nanowires could be attributed to the existence of a oxide layer surrounding Si nanowires and a cramped space for making ZnO branches which have the same or the larger diameter than the core Si nanowire. The oxide layer around core Si nanowires could be formed when the pressure was stabilized by making the balance between the gases flows(including oxygen gas) and the evacuation of the tube simultaneously and even with raising the temperatures. So these two factors (the oxygen flows and the cramped space of Si) could interrupt ZnO branches formation mainly.

The mean diameter of the ZnO branches formed into SnO_2 nanowires was around 20−30 nm, which showed the more uniform and stable formation of the hierarchical structures in Figure 5b-1 different to the case of Si nanowires of Figure 5a-1. The synthesis over 30 min induced merging of the nanostructures, as shown in the inset of Figure 5b-1. Fan et al. previously reported a sol−gel method for the fabrication of hierarchical structures with metal oxide materials,[7] but the secondary ZnO branches could not be formed without a ZnO seed layer. However, using our T-PLD technique, the secondary ZnO branches were easily grown on the SnO_2 backbone nanowires with no prior treatment. This was made possible by the plume particles having sufficient kinetic energy imparted by the pulsed laser and the hot furnace. This enabled effective dissolvableness and diffusion of the ZnO materials onto the SnO_2 surface and final nucleation of the feedstock to form the branch structure.

Figure 5a-2 shows an enlargement of the low-magnification TEM image of the Si-ZnO hierarchical structure. The diameter of the ZnO branch was almost 20−30 nm, and the crystalline branch was firmly attached to the Si backbone nanowire. The ZnO branches extended from the Si nanowires perpendicularly along the (002) *c*-axis of the ZnO Wurtzite structure with an interatomic distance of 0.5206 nm, as seen in TEM analysis of Figure 5a-3. The ZnO branches onto both the Si and SnO_2 nanowires were fabricated in T-PLD system without Au catalyst. Figure 5b-2 shows the low-magnification TEM image of the SnO_2−ZnO hierarchical structure. EDX analyses established that Sn, O, and Zn were at the center of the hierarchical structure, and only Zn and O were found in the branch area. The distribution of Zn surrounding the SnO_2 nanowire indicates the formation of the buffered ZnO layer before ZnO branches formation. Even though there is a publication which explain the detail for the cases of nanowires fabrication with or without a buffer layer according to the density of target materials or the ratio between elements of the target even the metal catalyst was used for the both cases, it seemed that it has to be studied more

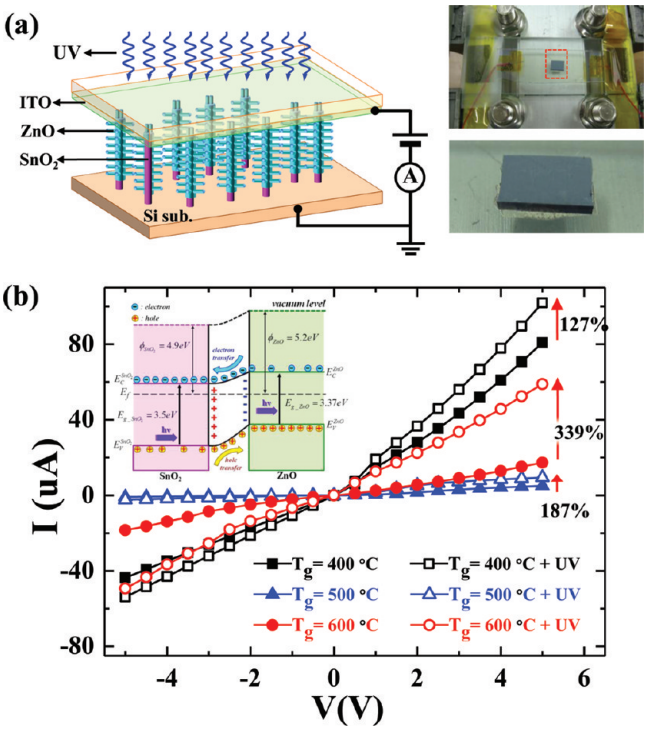

Figure 6. Schematic of the device with the SnO_2-ZnO hierarchical structure. (b) Voltage−current characteristics for the three kinds of SnO_2-ZnO hierarchical structures devices before and after UV irradiation (T_g = ZnO shell synthesis temperature by T-PLD)

specifically about the reason and the role of a buffer layer with Au catalyst in our T-PLD because there is not a system exactly same with this.[21] And the interatomic distance of the ZnO branch was 0.5206 nm in the SnO_2−ZnO hierarchical structures, as measured along the direction of the (002) *c*-axis of the general crystalline ZnO structure (Figure 5b-3). In Figure 6, the changes in the photocurrent in the SnO_2−ZnO hierarchical brush-shaped nanostructures were monitored under the illumination of 365-nm UV light. Short-wavelength UV light was selected to supply sufficient energy to create electron−hole pairs inside the ZnO materials having a band gap energy of 3.30 eV (376 nm) at 300 K. Figure 6a shows the SnO_2−ZnO hierarchical-structure devices made for photocurrent measurements. For transmission of the UV irradiation and electrical connection, the top electrode was fabricated with ITO glass and pressed down with the constant weight to ensure contact with the bottom-side SnO_2−ZnO hierarchical structures. ITO glass was well-known as a transparent conducting film in the visible light range and has adequate (80−90%) transmittance in the UV region.[22] The contact properties were shown as the ohmic with linear current−voltage characteristics. A voltage bias was applied to the SnO_2 nanowires from the bottom side of the heavily doped Si substrate, and the current was measured from the top side of the hierarchical structures through the transparent ITO glass, as shown schematically in Figure 6a. The photocurrents were measured for the devices having the SnO_2−ZnO hierarchical nanostructure synthesized at different temperatures.

When an active ZnO channel is irradiated with UV light there are not only the generation of electron−hole pairs but also the release of free carriers from the adsorbates on the ZnO surface. As previously studied, when the high energy of UV light or

electron beam irradiated onto the ZnO materials, the adsorbed water molecules or oxygen ions could be detached from the surface as releasing electrons to the channel as enhancing the conductance. Such improved photocurrent is usually attributed to the large portioned surface area to the volume in nanostructures. But in the investigation of the photocurrents in T-PLD grown heterostructures, the factors can be considered as the effective parameters for the enhancement of the conductance under the UV irradiation; the crystalinity of the ZnO structures, effective surface to volume ratio, etc. The photocurrents were measured and compared for three devices made by SnO_2−ZnO heterostructures synthesized at 400, 500, and 600 °C in the secondary growth of ZnO branches by T-PLD, as shown in Figure 6b. The relative increase of the photocurrent was improved as increasing the growth temperature of ZnO branches. The results were only compared with the increased portion of the conductance under the UV irradiation to the dark state current because there could be many factors which affect to the intrinsic electrical properties such as the different density of SnO_2 nanowires or the contact property between the structures and the top electrode. The largest relative increase (339%) was found for the hierarchical structures grown at 600 °C. And the heterostructures fabricated at T = 400 °C showed a relatively smaller photocurrent increase of 127%, attributed to the polycrystalline nature of the ZnO nanomaterials grown at low temperatures, as confirmed by the structural analysis shown in Figure 2a.

Our newly designed T-PLD system can produce hierarchical nanostructures having a good crystal quality using a pulsed laser generating a plasma plume and a hot furnace providing additional thermal energy. The shapes of ZnO materials formed on Si substrates by the T-PLD system as the one-step growth changed with the growth temperature; they were physically characterized by structural and spectroscopic analyses. By using two step growth by CVD and T-PLD, the SnO_2−ZnO heterostructures were also fabricated successfully as showing the large photocurrent in devices. We expect that our T-PLD growth method will be used to generate many different hierarchical heterostructures. These structures could be used as building blocks to form intrinsic p−n junction diodes, solar cells, and chemical sensors.

■ ASSOCIATED CONTENT

Supporting Information. As described in the manuscript, the all products synthesized by T-PLD in the one-step growth of ZnO at 200−700 °C were shown as SEM images, PL and XRD characteristics in the Supporting Information. And the peaks from the low temperature PL in ZnO nanoneedles grown at 600 °C were also represented. Finally, the SEM images of core−shell structures of Si−ZnO and SnO_2−ZnO could be found. This information is available free of charge via the Internet at http://pubs.acs.org/.

■ AUTHOR INFORMATION

Corresponding Author

*Tel: +82-31-330-4952 (C.U.J.); +82-2-3290-3250 (G.-T.K.). Fax; +82-31-330-4565 (C.U.J.); +82-2-953-3780 (G.-T.K.). E-mail: cu-jung@hufs.ac.kr (C.U.J.); gtkim@korea.ac.kr (G.-T.K.).

■ ACKNOWLEDGMENT

This research was supported by the National Research Foundation of Korea (NRF) funded by the Ministry of Education, Science, and Technology (2011K000623, R32-2011-000-10082-0, 20090066917, 20090084750).

■ REFERENCES

(1) Ahn, S. E.; Lee, J. S.; Kim, H.; Kim, S.; Kang, B. H.; Kim, K. H.; Kim, G. T. *Appl. Phys. Lett.* **2004**, *84*, 5022.
(2) Nakamura, T.; Yamada, Y.; Kusumori, T.; Minoura, H.; Muto, H. *Thin Solid Films* **2002**, *411*, 60.
(3) Ozgur, U.; Alivov, Y. I.; Liu, C.; Teke, A.; Reshchikov, M. A.; Dogan, S.; Avrutin, V.; Cho, S.-J.; Morkoc, H. *J. Appl. Phys.* **2005**, *98*, 041301.
(4) Tian, B.; Zheng, X.; Kempa, T. J.; Fang, Y.; Yu, N.; Yu, G.; Huang, J.; Lieber, C. M. *Nature* **2007**, *449*, 885.
(5) Hsueh, T.-J.; Hsu, C.-L.; Chang, S.-J.; Guo, P.-W.; Hsieh, J.-H.; Chen, I. C. *Scr. Mater* **2007**, *57*, 53.
(6) Hwang, I.-S.; Kim, S.-J.; Choi, J.-K.; Choi, J.; Ji, H.; Kim, G.-T.; Cao, G.; Lee, J.-H. *Sens. Actuators, B* **2010**, *148*, 595.
(7) Cheng, C.; Liu, B.; Yang, H.; Zhou, W.; Sun, L.; Chen, R.; Yu, S. F.; Zhang, J.; Gong, H.; Sun, H.; Fan, H. J. *ACS Nano* **2009**, 3, 3069.
(8) King, S. L.; Gardeniers, J. G. E.; Boyd, I. W. *Appl. Surf. Sci.* **1996**, *96*−*98*, 811.
(9) Hu, W. S.; Liu, Z. G.; Sun, J.; Zhu, S. N.; Xu, Q. Q.; Feng, D.; Ji, Z. M. *J. Phys. Chem. Solids* **1997**, *58* (6), 853.
(10) Loorenz, M.; Kaidashev, E. M.; Rahm, A.; Nobis, Th.; Lenzner, J.; Wagner, G.; Spemann, D.; Hochmuth, H.; Grundmann, M. *Appl. Phys. Lett.* **2005**, *86*, 143113.
(11) Kim, K.; Song, Y.-W.; Chang, S.; Kim, I.-H.; Kim, S.; Lee, S. Y. *Thin Solid Films* **2009**, *518*, 1190.
(12) Wu, Y.; Fan, R.; Yang, P. *Nano Letter.* **2002**, *2*, 83.
(13) Kim, G.-T.; Waizmann, U.; Roth, S. *Appl. Phys. Lett.* **2001**, *79*, 3497.
(14) Fujimura, N.; Nishihara, T.; Goto, S.; Xu, J.; Ito, T. *J. Cryst. Growth* **1993**, *130*, 269.
(15) Wagner, R. S.; Ellis, W. C. *Appl. Phys. Lett.* **1964**, *4*, 89.
(16) Sun, Y.; Fuge, G. M.; Ashfold, M. N. R. *Superlattices Microstruct.* **2006**, *39*, 33.
(17) Liu, X.; Wu, X.; Cao, H.; Chang, R. P. H *J. Appl. Phys.* **2004**, *95*, 3141.
(18) Vanheusden, K.; Seager, C. H.; Warren, W. L.; Tallant, D. R.; Voigt, J. A. *Appl. Phys. Lett.* **1996**, *68*, 403.
(19) Varshni, Y. P. *Physica.* **1967**, *34*, 149.
(20) Sakai, K.; Oyama, S.; Noguchi, K.; Fukuyama, A.; Ikari, T.; Okada, T. *Jpn. J. Appl. Phys.* **2009**, *48*, 085001.
(21) Yin, Y-.T.; Chen, Y-.Z.; Chen, C-.H.; Chen, L-.Y. *J. Chin. Chem. Soc.* **2011**, *58*, 5.
(22) Guillén, C.; Herrero, J. *Thin Solid Films* **2005**, *480*−*481*, 129.